(Revised MS to ES&T)

Reducing PAH Emissions from the Iron Ore Sintering Process by Optimizing Its Operation Parameters

Yu-Cheng Chen[1], *Perng-Jy Tsai*[1,2*], *Jin-Luh Mou*[3]

[1]Department of Environmental and Occupational Health, Medical College, National Cheng Kung University, 138, Sheng-Li Road, Tainan 70428, Taiwan

[2]Sustainable Environment Research Center, National Cheng Kung University, 1 University Road, Tainan 70101, Taiwan

[3]Department of Occupational Safety and Health, Chung Hwa University of Medical Technology, 89, Wenhwa 1st St., Rende Shiang, Tainan 71703, Taiwan

---

*__Correspondence author:__ Perng-Jy Tsai, Department of Environmental and Occupational Health, Medical College, National Cheng Kung University. 138, Sheng-Li Rd., Tainan 70428, Taiwan. Tel.: +886-6-2353535 ext. 5806; Fax: +886-6-2752484; E-mail address: pjtsai@mail.ncku.edu.tw

Running Title: Determining optimal operation condition for reducing PAH emissions in the iron ore sintering process by using Taguchi experimental design.

Abstract

This study was set out to reduce polycyclic aromatic hydrocarbon (PAH) emissions from the iron ore sintering process by optimizing its operation parameters obtained from the Taguchi experimental design. Four operating parameters, including the water content (Wc; range = 6.0−7.0 wt %), suction pressure (Ps; range = 1000−1400 mmH_2O), bed height (Hb; range = 500−600 mm) and type of hearth layer (HL; including sinter, hematite, and limonite) were selected and conducted on a pilot-scale sinter pot to simulate various sintering operating conditions of a real-scale sinter plant. We found that the resultant optimal combination (Wc = 6.5 wt%, Hb = 600 mm, Ps = 1400 mmH_2O, and HL = limonite) could reduce the emission factor of total BaP equivalent concentration (EF_{BaPeq}) up to 57.6% in comparison with the current operating condition of a real-scale sinter plant (Wc = 6.5 wt %, Hb = 550 mm, Ps = 1200 mmH_2O, and HL = sinter). Through the ANOVA analysis, we found that Ps and Hb were the top two parameters affecting total EF_{BaPeq} (accounting respectively for 70.9% and 21.2% of the total contribution of the four selected parameters). By examining both the sinter productivity and sinter strength, the values obtained from the optimal combination were quite comparable to those of the current operating condition. The above results further confirm the applicability of the obtained optimal combination for the real-scale sinter plant.

Keywords: PAH emission, iron ore sintering, operation parameters, optimal combination, Taguchi experimental design

Introduction

Polycyclic aromatic hydrocarbons (PAHs) and their derivatives could be formed during the incomplete and/or inefficient combustion of fossil fuels. PAHs are semi-volatile compounds presenting in the ambient air in not only the gas phase, but also the particulate phase through condensation or adsorption of gas-phase PAHs on the surface of particles (*1*). PAHs are known to be harmful to human health. Some PAHs, such as benzo[*a*]pyrene (BaP), and Cyclopenta[c,d]pyrene (CYC) and dibenz[*a,h*]anthracene (DBA), have been classified into *Group 1* and *Group 2A*, respectively, by the International Agency for Research on Cancer (IARC) (*2*). Many countries have also regulated the ambient air quality standards or proposed the limit value for the BaP (*3*). PAHs found in the outside ambient air can be generated both from the natural sources (such as forest fires and volcanic eruptions) and the anthropogenic sources (such as industrial combustion, traffic emission, and waste incineration) (*4*–*6*).

The iron and steelmaking is a highly energy-intensive process requiring burning of fossil fuels, including coal and coke and is known as one of the significant PAH emission sources (*7*–*9*). As reported by Ravindra et al., (*3*) and Bjøresth and Ramdahl (*10*) studies, PAHs emitted from iron and steel industries have been recognized as the second major source in Europe, accounting for 12.0–20.2% of yearly total PAH emissions. In an integrated iron and steel plant, the iron ore sintering process plays an important role on PAH emissions due to its extremely large flue gas volume. Iron ore sintering is an agglomeration process to convert iron ore fines (raw mixture) into lumpy agglomerates. In the preliminary stage of sinter making process, water was sprayed onto the raw mixtures in the mixing drum to increase the granular sizes for enhancing the permeability of the sinter bed. During sintering, the raw mixtures were first ignited by gas-fueled (nature gas) burns situated at the beginning of the steel belt conveyer. Then, the sinter bed was heated to temperature of ~1000 ºC or above. Suction air passes through the sinter layer by means of wind legs and a fan, which moves the melting/combustion zone to the down layer to produce sintered products.

The sintering process has been developed for several decades in the iron and steel manufacturing industry. Traditionally, air pollution control devices (APCDs) for the control of PAH emissions have been widely used to reduce their environmental impacts. Nevertheless, most sinter plants have faced the dilemma regarding how to continuously upgrade their APCDs in order to comply with stricter and stricter emission standards adopted in their countries. In order to comply with future PAH emission standard and decrease the cost resulting from upgrading the end-pipe PAH control devices, it is important to develop an effective method for directly reducing PAH generations during the sintering process. Therefore, to optimize operating conditions in order to reduce PAH formations via oxidation reaction might provide a promising solution. In addition to the property of the sinter raw mixture, the four operating parameters, including the water content (Wc), suction pressure (Ps), bed height (Hb) and type of hearth layer (HL), are major factors affecting combustion conditions during the iron ore sintering process (*11-13*). Among these four parameters, the content of Wc in the sinter bed might affect the adsorption of PAHs on the surface of particles and the solubility of PAHs in water or might affect the heating value of coke in combustion; the magnitude of Ps affects the air (or oxygen) supply which might play an important role in the oxidation reaction related to PAH formations (*14*); Hb affects the thickness and temperature profile of the combustion zone of the sinter bed and in consequence affects the contents of unburned hydrocarbon compounds during the sintering process (*15*); and the type of the HL might affect the catalytic oxidation reaction associated with PAH formations (*13, 16*). All these operating parameters have been used to control the structure of the sinter bed to simulate various operation conditions for the sintering process in many studies (*11, 17–19*). It is known that the cost reduction and the sinter production are the major concerns of the real-scale sinter plant rather than PAHs reduction. As a result the selected iron ores might come from numerous mine sources because of cost and quality considerations and result in considerable variations in the contents of the sintering raw mixture. Therefore, it would become impractical for changing the contents of the sintering raw mixture in a real-scale sinter plant simply for reducing its PAH emissions. Therefore, to seek for an optimal combination of Wc, Ps, Hb and HL for reducing PAH formations during the sintering process might provide a promising solution.

In this study the Taguchi experimental design was used to determine the optimal operating combination for reducing PAH formations during the sintering process. In addition, two important indexes (i.e. the sinter productivity and sinter strength) widely used for characterizing the quality of the sintering products were also examined to further ensure the optimal combination obtained from the Taguchi experimental design can be used in the real-scale sinter plant.

Material and Methods

The Pilot Scale Sinter Pot and Its Operating Procedures. A pilot scale sinter pot was used in this study to simulate the real-scale sintering process (Fig. 1). It has been wildly used in pilot tests for iron ore and steel industries for improving their sinter production (*12, 20*) and the control of their emitted air contaminants (such as PCDD/Fs) (*21, 22*), although the volume of this sinter pot (0.051 m^3) is quite small as in comparison with the real-scale sinter plant (400 m^3). This sinter pot included a pot body (inner diameter = 330 mm, height = 600 mm), an ignition hood, and a windbox connected to an exhaust duct. Six kilogram of hearth layer (particle diameters = 10–15 mm, thickness = 40 mm) were placed inside the sinter pot. The temperature profiles and related chemical reactions that presumably occurred in the sinter pot during combustion were also illustrated in Fig. 1. Results associated with the zone combustion process of the sinter pot have been described in details in the previous studies (*21–22*). Outlet gas temperature was measured by three type-k thermocouples located in the windbox to monitor sintering scenario during the combustion process. During sintering, the designated ignition temperature in ignition hood was specified at 1150–1200 ℃ for 1.5 min and then held in another 1.5 min for keeping heat. During this period (i.e., starting from the ignition to the removal of the ignition hood) the suction pressure inside the sinter pot was controlled at 800 mmH_2O by using an electromagnetic valve. After this, the suction pressure was raised to 1200 mmH_2O and then kept constant throughout the end of the sintering process. The total sintering time was around 35 min depending on the experimental conditions.

The sintering raw mixture used in this study was directly obtained from the real-scale sinter plant. Its contents and the analyzed chemical compositions show in Table 1.

The Taguchi Experimental Design. The Taguchi experimental design is a powerful tool that provides a simple, efficient and systematic approach to optimize operating conditions under designated ranges of all selected parameters. The details of the Taguchi experimental design can be seen in the Supporting Information (SI). The working steps for the Taguchi experimental design include: (1) selection of operation parameters; (2) determination of the number of levels for each selected parameter; (3) selection of the appropriate orthogonal array and arrangement of operation parameters to the orthogonal array; (4) conducting experiments based on the arrangement of the orthogonal array; (5) analysis of the experimental results using the S/N ratio and ANOVA analyses; (6) selection of the optimal combination of levels for the selected operation parameter; and (7) verification of the above optimal combination by conducting a confirmation experiment (*23*, *24*).

Selected Operation Parameters, Levels and Orthogonal Array. Four operation parameters (and their testing ranges), including water content (Wc; 6.0–7.0 wt %), suction pressure (Ps; 1000–1400 mm H_2O), bed height (Hb; 500–600 mm), and types of hearth layer (HL; including sinter (containing 70% Fe_2O_3 and 7% Fe_3O_4; Fe in total accounting for 58.1% of total weight), hematite (containing 88% Fe_2O_3 and 7% FeO·OH; Fe in total accounting for 64.1% of total weight), and limonite (containing 40% Fe_2O_3, 45% FeO·OH and 6% H_2O; Fe in total accounting for 63.3% of total weight)) were selected in this study. The selected ranges of the above four parameters were determined based on the past operation experience of the selected sinter plant and the published references (*17, 25–26*). A specific combination of the four selected operation parameters (i.e., Wc = 6.5 wt %, Ps = 1200 mmH_2O, Hb = 550 mm, and type of HL = sinter) being currently used in the real-scale sinter plant was served as the reference combination. SI Table S1 shows the selected three levels for each operation parameter based on its designated range. SI Table S2 shows an *L9(3^4)* orthogonal array (with four columns and nine rows) used in this study according to the Taguchi experimental design (*23*). Since the experimental design was orthogonal, it was possible to discriminate the effect of each individual parameter at each designated level. As shown in SI Table S2, nine combinations of the four selected operation parameters were chosen for conducting experiments. Subjected to the cost associated with samplings, sample analyses and sinter pot operation, each experiment were repeated twice (n = 2) in this study.

PAH sampling. For each experiment, the flue gas samples were collected from the duct located at the downstream of the windbox of the pilot sinter pot (see Fig 1) by using a PAHs Sampling System (PSS; Li-The Co., Kaoushing, Taiwan) (*27*). Because the instability of the airstream occurred during the first five minutes of the sintering process (i.e., the time needed for adjusting the suction pressure to reach the designated level), the flue gas of the first five minute was not collected. As a result, the sampling time for each flue gas sample was ~30 min. During sampling, the flue gas (including particle- and gas-phase PAHs) was sampled iso-kinetically throughout each batch sintering. The details of the PAH sampling method can be seen in the SI.

PAH analysis. For each collected sample, both its glass fiber filter and PUF/resin cartridge were Soxhelt extracted in a mixed solvent (n-hexane and dichloromethane v:v = 1:1) for 24 hours. The extract was concentrated by purging with ultra-pure nitrogen to 2 ml, cleaned-up and then re-concentrated to exactly 1.0 ml. The contents of 22 PAH compounds were determined by using a gas chromatograph with a mass selective detector (GC/MS) and a computer work station. Detailed analytical methods and conditions were included in the SI or presented in our previous works (27–*28*).

Evaluation of Sinter Productivity and Sinter Strength. The sinter productivity, expressed in tons per square meter of grate area of sintering machine per day, was calculated from the sintering time, the cross-sectional area of the pot grate, and the weight of sinter product recovered from the test (by removing the loss of the weight of hearth layer). The sinter strength was measured by using a modified ISO 3271 test method (*29*).

Data Analysis. In this study, the total PAH concentration was defined as the sum of the concentrations of the selected 22 PAH compounds. In addition, PAH contents were further divided into three categories (LMW-, MMW- and HMW-PAHs) according to their molecular weights (see in SI Table S3).

Because BaP has been known to be the most carcinogenic PAH compound, the carcinogenic potency of each collected sample was also determined in terms of its BaP equivalent concentration (BaP_{eq}). To calculate the BaP_{eq} for each individual PAH species, it requires the use of its toxic equivalent factor (TEF) for the given species relative to BaP carcinogenic potency. Each selected TEF corresponding it's PAH compound has been reported by our previous works (*27, 30*). The carcinogenic potency of the total BaP_{eq} was estimated as the sum of individual BaP_{eq} of the 22 PAH compounds. In the present study, considering the variations in flow rate, sintering time, and charging weight of feedstock among different experimental combinations, the emission factor of total BaP_{eq} (EF_{BaPeq}; μg/kg-feedstock) was calculated to compare for reducing the environmental impact purpose. The details associated with the calculation of EF_{BaPeq} can be seen in the SI.

The S/N ratio based on the concept of the-lower-the-better was used to characterize EF_{BaPeq}. The details of the calculated equations including the S/N ratio and its predicted value for the optimal combination can be seen in the SI. In addition, the analysis of variance (ANOVA) was used to investigate the effect of each individual parameter on EF_{BaPeq}.

Results and Discussion

Concentrations and Characteristics of PAHs Emitted from the Sintering Process. The SI Figure S1 shows the fractions of 22 PAHs (mean and range) obtained from each of the nine selected experimental combinations as using Test A-sintering raw mixture. The most abundant PAHs presented in sequence were NaP, AcPy, Flu, PA and Acp. Table 2 further classifies the above concentrations into LMW-, MMW-, and HMW-PAHs, gas- and particle-phase PAHs, total PAH, and total BaP_{eq}

concentrations. The mean total PAH and BaP_{eq} concentrations were 504 μg/Nm^3 (range = 355–673 μg/Nm^3) and 5.35 μg/Nm^3 (range = 2.80–7.41 μg/Nm^3), respectively. The total PAHs was mostly contributed by gas-phase PAHs (mean = 479 μg/Nm^3) accounting for 95.1% (range = 93.2–97.7%) emissions of total PAHs. The LMW-PAHs was the most dominant PAH homologue (mean = 473 μg/Nm^3) accounting for 93.8% (range = 90.9–94.6%) emissions of total PAHs. Because of the high volatility of LMW-PAHs, the above results further confirm that most PAHs were in the form of the gas phase. In contrast, the MMW- and HMW-PAHs, although were know with higher carcinogenic potencies, were the least and second least dominant homologues (mean = 10.3 and 20.8 μg/Nm^3, respectively) accounting respectively for 2.04% and 4.13% (range = 1.53–2.85% and 3.12–6.52%, respectively) emissions of total PAHs. Table 2 also shows the emission factor of total BaP_{eq} (total EF_{BaPeq}) for each combination. We found that the mean total EF_{BaPeq} for the nine selected experimental combinations was 23.4 μg/kg-feedstock (range = 10.9–34.2 μg/kg-feedstock). Due to the intrinsic differences in flow rate, sintering time and charging weight of the nine selected experimental combinations, it should be noted that the trend in magnitude of total EF_{BaPeq} was somewhat different from that of total BaP_{eq} concentrations. The above result clearly indicates the importance of using total EF_{BaPeq} to determine the optimal combination for reducing PAH emissions from the sintering process.

Comparison of PAH Characteristics and Concentrations between This Sinter Pot and Sinter Plants. Table 3 shows PAH characteristics (including profile, homologue distributions, particle- (sinter pot = 4.3%; sinter plant = 6.7%) and gas-phase (sinter pot = 95.7%; sinter plant = 86%) distribution) and concentrations (including mean total concentration (sinter pot = 504 μg/Nm^3; sinter plant = 778 μg/Nm^3) and EF_{PAHs} (sinter pot = 2364 μg/kg-feedstock; sinter plant = 3160 μg/kg-feedstock)) obtained from the present study and real-scale sinter plants (*7, 31*). We found above both results were comparable indicating our results could be representative of iron metallurgy.

S/N Ratios and ANOVA Analysis. In this study, the total EF_{BaPeq} obtained from the nine selected experimental combinations were used to calculate S/N ratio. The S/N ratios of the four selected parameters in three designated levels according to the orthogonal array of the experimental arrangement were presented in SI Table S4. We found that the resultant S/N ratios fell to the range from –20.5 to –29.7 dB. SI Table S5 shows mean S/N ratios of the four selected parameters in each of their three designated levels. For each selected parameter, the difference between maximum S/N ratio and its corresponding minimum S/N ratio (i.e., max–min) represents the effect of the given parameter on determining total EF_{BaPeq}. Based on this, we found that the effects in sequence for the four selected parameters on total EF_{BaPeq} were: Ps (5.29 dB), Hb (3.07 dB), HL (1.14 dB) and Wc (0.81 dB). Figure 2 shows the trend of the resultant S/N ratios for each selected parameters at the three designated levels affecting total EF_{BaPeq}. Both Ps and HL shared the same trend in their resultant S/N ratios (i.e., first decreased then increased). The above trend was different from that of Wc (i.e., first increased then decreased) and Hb. The combination of Wc (= 6.5 wt %), Ps (= 1400 mmH_2O), Hb (= 600 mm), and HL (= limonite) were found with the highest S/N ratio for each of the four selected parameters, and hence was considered as the optimal operation condition for reducing PAH emissions.

In this study, the ANOVA analysis was used to prioritize effects of the four selected parameters on determining total EF_{BaPeq}. The result shows that Ps ($p < 0.01$) and Hb ($p = 0.021$) were the significant parameters accounting for 70.9% and 21.2%, respectively, of the total contribution of the four selected parameters (SI Table S6). The above result was consistent with that found in previous studies (*14, 15, 19, 32*). Thomas et al., (*14*) and Ledesma et al. (*32*) have indicated that PAH compounds decreased at high oxygen concentrations (i.e. high air supply passing through combustion zone during sintering process), in accordance with their destruction by oxidation. The high Hb was close to ignition hood that might result in a wider melting/combustion zone in the sinter bed, leading to more complete coke combustion and less PAH formations during the sintering process (*15, 19*). For the result of Wc, although the effect was not significance ($p = 0.665$), it should be noted that the optimal Wc found at the middle level (i.e., 6.5 wt %) might be worth further discussion. Kasai et al. (*33*) and Haga et al. (*34*) have indicated that the increase of Wc in sinter raw mixtures could increase the permeability of sintering bed and combustion efficiency (due to the abundant coke breezes and limestone fines coating on the surface of particles), and hence results in reducing PAH formations during sintering processes. On the other hand, Gulyurtlu et al. (*35*) have indicated that the high level of water content could result in local quenching of the combustion reactions, which in turn could lead to PAH formations. Based on these, it is not so surprising to see that the lowest total EF_{BaPeq} was found at the middle level (i.e., 6.5 wt %) rather than at 6.0 wt % or 7.0 wt %. For the type of HL, we found that the use of limonite could slightly decrease total EF_{BaPeq} in comparison with the use of sinter as the HL of the sinter pot, although the above effect was not significance (p = 0.467). Cieplik et al. (*13*) have indicated that limonite could exhibit higher potent catalytic activity of oxidation than that of hematite. However, Guélou et al. have reported that Fe content might play an important role in catalytic oxidation of carbon monoxide, and the higher Fe content might result in the less PAH formations (*36*). The above inference is consistent with what we have found in the three selected types of HL in their Fe contents (i.e., hematite (64.1%) ≅ limonite (63.3%) > sinter (58.1%)). Nevertheless, the insignificant effect associated with the types of HL used in this study might mainly because the depth of the HL was too thin to have sufficient reaction time for the formation of PAHs during sintering process. In addition, it should be noted that other physical parameters of HL, such as the particle size and porosity, could also be important factors affecting PAH formations. Therefore, the net effect of HL on PAH formations warrants the needs for further research in the future.

Comparison PAH emissions between the Reference and the Optimal Operation Combination. Table 4 shows the total EF_{BaPeq} and the S/N ratio obtained from the reference combination (i.e, Wc = 6.5 wt %, Ps = 1200 mmH_2O, Hb = 550 mm, and HL = sinter) and the resultant optimal combination (i.e., Wc = 6.50 w%, Ps = 1400 mmH_2O, Hb = 600 mm, and HL = limonite). The total EF_{BaPeq} and its corresponding S/N ratio for the reference combination were found as 28.6 μg/kg-feedstock and −29.1 dB, respectively. For the predicted optimal combination, its total EF_{BaPeq} and S/N ratio (predicted based on the SI eq 4) were found as 10.9 μg/kg-feedstock and −20.5 dB, respectively. The difference in the above two S/N ratios (= 8.6 dB) indicating that the use of the optimal combination would result in a decrease in total EF_{BaPeq} up to 61.9% in comparison with the reference combination. For confirmation purpose, experiments (n = 2) were conducted as using Test B-sintering raw mixture based on the specification of the reference combination and the resultant optimal combination. The resultant mean total EF_{BaPeq} obtained from the reference combination and the confirmation combination were found as 60.3 and 25.6 μg/kg-feedstock, respectively (Table 4). The decrease EF_{BaPeq} from the reference combination to the optimal combination (confirmation experiments) was up to 57.6% (range = 54.3–60.8%). The above similar decreases in total EF_{BaPeq} further confirm the applicability of the obtained optimal combination for reducing PAH formations during the sintering process.

Figure 3 shows PAH concentrations (including 2- to 7-ringed PAHs, and LMW- MMW- and HMW-PAHs in the particle- and gas-phase, respectively) obtained from the sinter pot operated under the reference combination and the optimal combination for the confirmation purpose. While operated under the optimal combination, gas-phase MMW- and HMW-PAH concentrations decreased significantly (= 72.9% and 67.4%, respectively) in comparison with that of the reference combination. In contrast, gas-phase LMW-PAHs increased up to 31.2%. The above results might be because MMW- and HMW-PAHs were much easier to be cleaved into LMW-PAHs under the optimal combination than that of the reference combination. For particle-phase PAHs, all selected PAH homologues (particularly for HMW-PAHs) decreased consistently from the optimal to the reference combination. The above results indicate that the use of the optimal combination could significantly reduce high molecular weight PAH formations. Considering the formation mechanisms HMW-PAHs were similar to those of PCDFs during the sintering process (*37*), our results might provide another solution to suppress PCDD/F formations in the future.

Sinter Productivity and Sinter Strength of the Reference and Optimal Operation Combination. Although the resultant optimal combination was able to reduce PAH emissions, it is important to examine its impact on the sinter productivity and sinter strength for practical reason. In this study, we found that the sinter productivity and sinter strength for the reference combination were 38.9 t/m^2/day and 71.1%, respectively. The above values were quite comparable to those found for the optimal combination (=39.5 t/m^2/day and 70.2%, respectively). Therefore, it is concluded that the use of the optimal combination determined by the Taguchi experimental design for the sintering process could effectively reduce PAH emissions without interfering with the quantity of its sinter products.

Acknowledgements

We thank the China Steel Corporation (CSC) in Taiwan for funding this research project. We also thank the staffs at CSC for providing testing materials and facilities.

Supporting Information Available

Information about the details of Taguchi experimental design, sampling and analytical methods, conditions, data analysis, six additional tables and one figure. This material is available free of charge via the Internet at http://pubs.acs.org.

Literature Cited

(1). Coutant, R. W.; Brown, L.; Chuang, J. C.; Riggin, R. M.; Lewis, R. G. Phase distribution and artifact formation in ambient air sampling for polynuclear aromatic hydrocarbons. *Atmos. Environ.t* **1988**, *22*, 403–409.

(2). International Agency for Research on Cancer (IARC), Vol. 92 (in preparation), Polycyclic Aromatic Hydrocarbons: Summary of Data Reported and Evaluation **2007**. http://monographs.iarc.fr/ENG/Meetings/92-pahs.pdf.

(3). Ravindra, K.; Sokhi, R.; Grieken, R. V. Atmospheric polycyclic aromatic hydrocarbons: Source attribution, emission factors and regulation. *Atmos. Environ.* **2008**, *42,* 2895–2921.

(4). Marr, L. C.; Kirchstetter, T. W.; Harley, R. A.; Miguel, A. H.; Hering, S. V.; Hammond, S. K. Characterization of Polycyclic Aromatic Hydrocarbons in Motor Vehicle Fuels and Exhaust Emissions. *Environ. Sci. Technol.* **1999**, *33*, 3091–3099.

(5). Omar, N. Y. M. J., Abas, M. R. B., Ketuly, K. A., Tahir, N. M. Concentrations of PAHs in atmospheric particles (PM-10) and roadside soil particles collected in Kuala Lumpur, Malaysia. *Atmos. Environ.* **2002**, *36*, 247–254.

(6). Dyke, P. H.; Foan, C.; Fiedler, H. PCB and PAH releases from power stations and waste incineration processes in the UK. *Chemosphere* **2003**, *50*, 469–480.

(7). Yang, H. H.; Lai, S. O.; Hsieh, L. T.; Hsueh, H. J.; Chi, T. W. Profiles of PAH emission from steel and iron industries. *Chemosphere* **2002**, *48*, 1061–1074.

(8). Almaula, S. Polycyclic Aromatic Hydrocarbons from Steelmaking. *Environ. Forensics* **2005**, *6*, 143–150.

(9). Tsai, J. H.; Lin, K. H.; Chen, C. Y.; Ding, J. Y.; Choa, C. G.; Chiang, H. L. Chemical constituents in particulate emissions from an integrated iron and steel facility. *J. Hazard. Mater.* **2007**, *147*, 111–119.

(10). Bjorseth A.; Ramdahl T. *Handbook of Polycyclic Aromatic Hydrocarbons*; Marcel Dekker: New York, 1985.

(11). Maeda, T.; Fukumoto, C.; Matsumura, T.; Nishioka, K.; Shimizu, M. Effect of adding moisture and wettability on granulation of iron ore. *ISIJ Int.* **2005**, *45*, 477–484.

(12). Kamijo, C.; Matsumura, M.; Kawaguchi, T. Sintering behavior of raw material bed placing large particles. *ISIJ Int.* **2005**, *45*, 544–550.

(13). Cieplik, M. K.; Carbonell, J. P.; Munoz, C.; Baker, S.; Kruger, S.; Liljelind, P.; Marklund, S.; Louw, R. On Dioxin Formation in Iron Ore Sintering. *Environ. Sci. Technol.* **2003,** *37*, 3323–3331.

(14). Thomas S.; Wornat M. J. The effects of oxygen on the yields of polycyclic aromatic hydrocarbons formed during the pyrolysis and fuel-rich oxidation of catechol. *Fuel* **2008**, *87*, 768–781.

(15). Mitterlehner, J.; Loeffler, G.; Winter, F.; Hofbauer, H.; Schmid, H.; Zwittag, E.; Buergler, T. H.; Pammer, O.; Stiasny, H. Modeling and simulation of heat front propagation in the iron ore sintering process. *ISIJ Int.* **2004,** *44*, 11–20.

(16). Imai, T.; Matsui, T.; Fujii, Y.; Nakai, T.; Tanaka, S. Oxidation catalyst of iron oxide suppressing dioxin formation in polyethylene combustion. *J. Mater. Cycles. Waste. Manag.* **2001**, *3*, 103–109.

(17). Nath, N. K.; Mitra, K. Optimisation of suction pressure for iron ore sintering by genetic algorithm. *Ironmak. Steelmak.* **2004**, *31*, 199–206.

(18).Kawaguchi, T.; Kamijo, C.; Matsumura, M. The sintering behavior of raw material bed placing large particles. *Tetsu to Hagane* **2006**, *92*, 779–787.

(19).Yang, W.; Choi, S.; Choi, E. S.; Ri, D. W.; Kim, S. Combustion characteristics in an iron ore sintering bed–evaluation of fuel substitution. *Combust. Flame* **2006**, *145*, 447–463.

(20).Higuchi, K.; Kawaguchi, T.; Kobayashi, M.; Hosotani, Y.; Nakamura, K.; Iwamoto, K.; Fujimoto, M. Improvement of Productivity by Stand-support Sintering in Commercial Sintering Machines, *ISIJ Int.* **2000**, 40, 1188–1194.

(21).Kasai, E.; Harjanto, S.; Terui, T.; Nakamura, T.; Waseda, Y. Thermal remediation of PCDD/Fs contaminated soil by zone combustion process, *Chemosphere* **2000**, *41*, 857–864.

(22).Harjanto, S.; Kasai, E.; Terui, T.; Nakamura, T. Formation and transport of PCDD/Fs in the packed bed of soil containing organic chloride during a thermal remediation process, *Chemosphere* **2002**, *49*, 217–224.

(23).Taguchi, G. *Introduction to quality engineering: designing quality into products and processes*; Asian Productivity Organization: Tokyo, Japan, 1987.

(24).Yang, W. H.; Tarng, Y. S. Design optimization of cutting parameters for turning operations based on the Taguchi method. *J. Mater. Process. Tech.* **1998,** *84*, 122–129.

(25).Yang, W.; Ryu, C.; Choi, S.; Choi, E.; Lee, D.; Huh, W. Modeling of combustion and heat transfer in an iron ore sintering bed with considerations of multiple solid phases. *ISIJ Int.* **2004**, *44*, 492–499.

(26).Oyama, N.; Sato, H.; Takeda, K.; Ariyama, T.; Masumoto, S.; Jinno, T.; Fujii, N. Development of coating granulation process at commercial sintering plant for improving productivity and reducibility. *ISIJ Int.* **2005**, *45*, 817–826.

(27).Chen, Y. C.; Lee, W. J.; Uang, S. N.; Lee, S. H.; Tsai, P. J. Characteristics of polycyclic aromatic hydrocarbon (PAH) emissions from a UH-1H helicopter engine and its impact on the ambient environment. *Atmos. Environ.* **2006**, *40*, 7589–7597.

(28).Tsai, P. J.; Shih, T.S.; Chen, S. L.; Lee, W. J.; Lai, G. H.; Liou, S. H. Assessing the contents of polycyclic aromatic hydrocarbons in the tollbooths of a highway toll station via direct and indirect approaches. *Environ. Sci. Technol.* **2002**, *36*, 4748–5473.

(29).Iron ores – Determination of tumble strength, 3rd ed.; International Organization for Standardization (ISO) 3271: Geneva, 1995.

(30).Tsai, P. J.; Shih, T. S.; Chen, S. L.; Lee, W. J.; Lai, G. H.; Liou, S. H. Assessing and Predicting the Exposures of Polycyclic Aromatic Hydrocarbons (PAHs) and Their Carcinogenic Potencies from Vehicle Engine Exhausts to Highway Toll Station Workers. *Atmos. Environ.* **2004**, *38*, 333–343.

(31).Ooi, T. C.; Aries, E.; Ewan, B. C. R.; Thompson, D.; Anderson, D. R.; Fisher, R.; Fray, T.; Tognarelli, D. The study of sunflower seed husks as a fuel in the iron ore sintering process. *Miner. Eng.* **2008**, *21*, 167-177.

(32).Ledesma, E. B.; Kalish, M. A.; Nelson, P. F.; Wornat, M. J.; Mackie, J. C. Formation and fate of PAH during the pyrolysis and fuel-rich combustion of coal primary tar. *Fuel* **2001**, *35*, 1801–1814.

(33).Kasai, E.; Rankin, W. J.; Gannon, J. F. The effect of raw mixture properties on bed permeability during sintering. *ISIJ Int.* **1989**, *29*, 33–42.

(34).Haga, T.; Ohshio, A.; Nakamura, K.; Kozono, T. Control technique of the melting reaction in sintering process by the fine part selective granulation of clayish iron ores. *Tetsu to Hagane* **1997**, *83*, 103–108.

(35).Gulyurtlu, I.; Karunaratne, D. G. G. P.; Cabrita, I. The study of the effect of operating parameters on the PAH formation during the combustion of coconut shell in a fluidised bed. *Fuel* **2003**, *82*, 215–223.

(36).Guélou, E.; Barrault, J.; Fournier, J.; Tatibouët, J. M. Active iron species in the catalytic wet peroxide oxidation of phenol over pillared clays containing iron. *Appl. Catal. B-Environ.* **2003**, *44*, 1–8.

(37).Iino, F.; Imagawa, T.; Takeuchi, M.; Sadakata, M. De novo synthesis mechanism of polychlorinated dibenzofurans from polycyclic aromatic hydrocarbons and the characteristic isomers of polychlorinated naphthalenes. *Environ. Sci. Technol.* **1999**, *33*, 1038–1043.

Brief: Using the Taguchi experimental design to identify the optimal operating condition provides useful approaches for reducing PAH formations during the iron ore sintering process.

Captions

Figures

FIGURE 1. The schematic of the pilot scale sinter pot and the illustration of its zone combustion process

FIGURE 2. Mean S/N ratios of the four selected operation parameters at the three designated levels

FIGURE 3. PAH concentrations (including 2- to 7-ringed PAHs, and LMW- MMW- and HMW-PAHs in the particle- and gas-phase, respectively) obtained from the sinter pot operated under the reference combination and the optimal combination for confirmation purpose

Tables

TABLE 1. The contents of sintering raw mixture and its chemical compositions in Test A and Test B

TABLE 2. The mean (range) of LMW-, MMW-, and HMW-PAHs, gas- and particle-phase PAHs, total PAH, and total BaP_{eq} emission concentrations (μg/Nm^3) in the flue gas of the nine designed experimental combinations and their corresponding emission factors of total BaP_{eq} (EF_{BaPeq}; μg/kg-feedstock)

TABLE 3. The comparison of PAH profiles, homologues, gas- and particle-phase distributions (range), mean (range) total concentration and EF_{PAHs} obtained from the present study with those data collected from real-scale sinter plants.

TABLE 4. The emitted total EF_{BaPeq} (μ g/kg-feedstock) and its corresponding S/N ratio (dB) obtained from the reference operation combination and optimal operation combination (including both predicted and that obtained from the confirmation experiments)

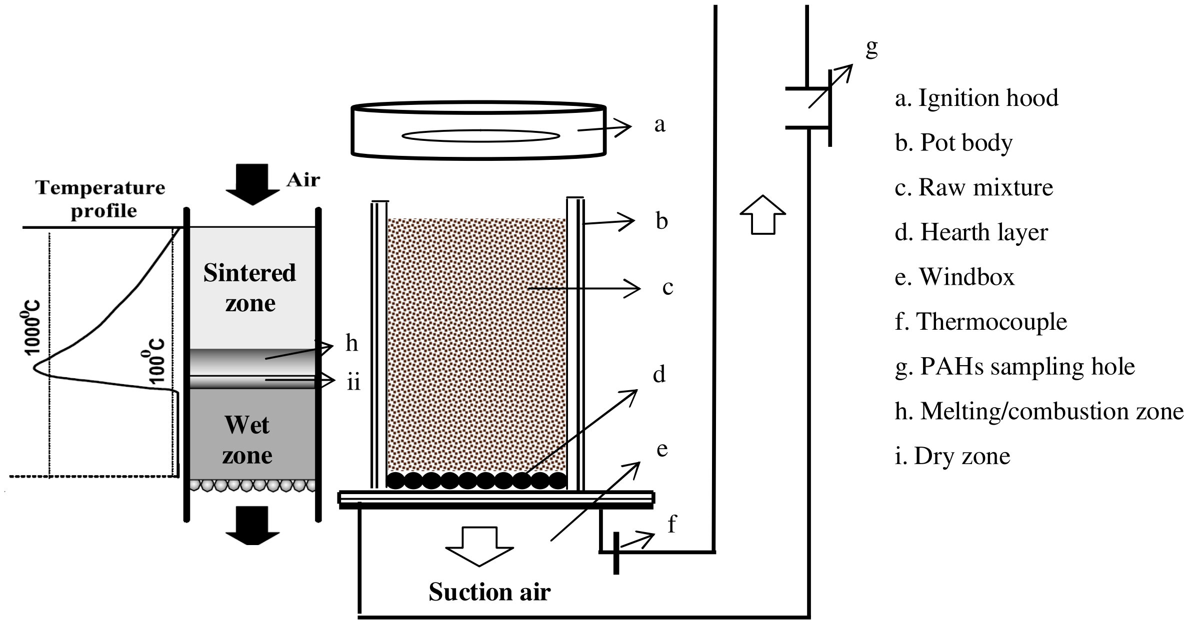

FIGURE. 1 The schematic of the pilot scale sinter pot and the illustration of its zone combustion process

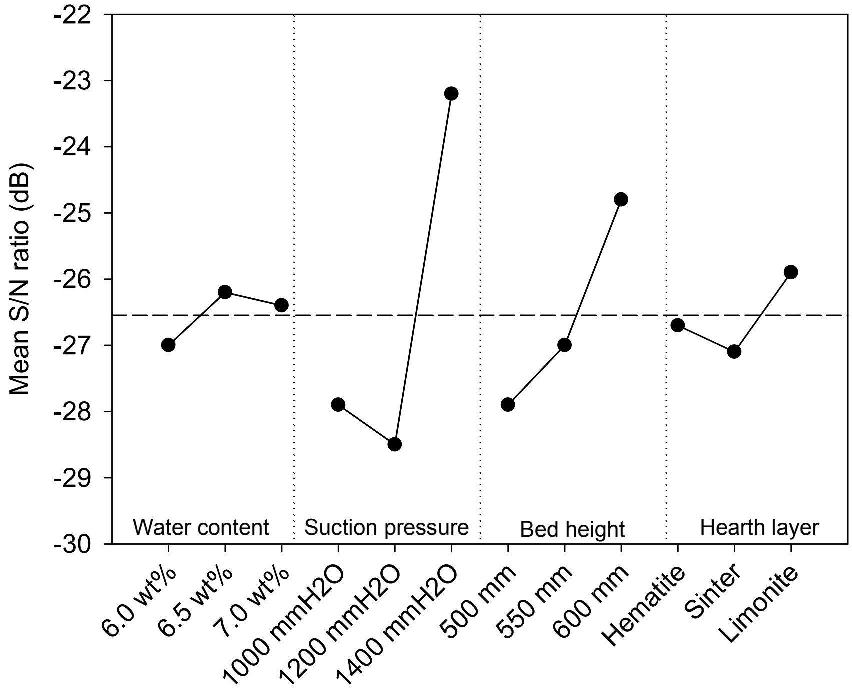

FIGURE 2 Mean S/N ratios of the four selected operation parameters at the three designated levels

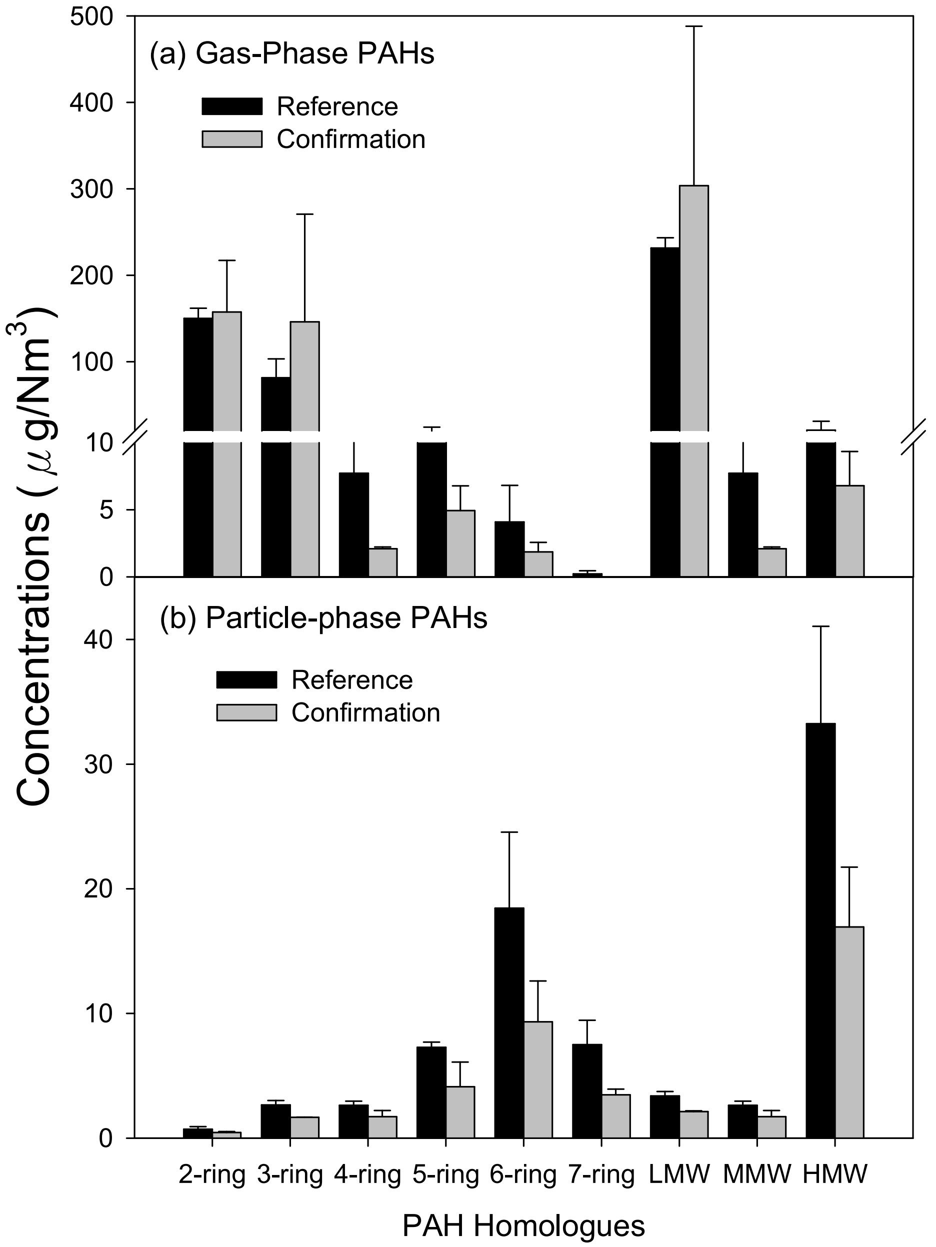

FIGURE 3 PAH concentrations (including 2- to 7-ringed PAHs, and LMW- MMW- and HMW-PAHs in the particle- and gas-phase, respectively) obtained from the sinter pot operated under the reference combination and the optimal combination for confirmation purpose

Table 1. The contents (wt %) of sintering raw mixture and its chemical composition (wt %)in Test A and Test B

Raw mixture	iron ore	coke breeze	anthracite	serpentine	marble	slurry	return fine[a]	Mini-pellet
Test A	52.8	3.99	1.84	0.421	1.98	0.562	31.5	1.50
Test B	61.1	1.88	1.92	0.647	2.94	0.888	30.4	0.241
Chemical composition	CaO	MgO	Al_2O_3	SiO_2	FeO	Total-Fe		
Test A	9.38	1.44	1.66	4.79	8.51	57.5		
Test B	9.31	1.16	1.80	2.80	6.72	58.2		

[a] including return fine obtained from sinter plant and blast furnace; Test A: prediction experiments; Test B: confirmation experiments

Table 2. The mean (range) of LMW-, MMW-, and HMW-PAHs, gas- and particle-phase PAHs, total PAH, and total BaP_{eq} emission concentrations (μg/Nm^3) in the flue gas of the nine designed experimental combinations and their corresponding emission factors of total BaP_{eq} (EF_{BaPeq}; μg/kg-feedstock)

emission concentration	experimental combination									mean
	1	2	3	4	5	6	7	8	9	
LMW-PAHs	372 (349–395)	595 (485–704)	356 (285–427)	497 (458–536)	379 (332–425)	334 (324–344)	536 (519–552)	554 (528–579)	632 (627–636)	473 (334–632)
MMW-PAHs	10.7 (8.89–12.5)	9.79 (8.20–11.4)	9.52 (3.72–15.3)	8.12 (7.08–9.17)	7.69 (4.74–10.6)	5.70 (4.87–6.54)	12.4 (3.13–21.8)	9.94 (3.95–15.9)	19.2 (16.1–22.2)	10.3 (5.70–19.2)
HMW-PAHs	26.7 (23.9–29.5)	24.3 (22.3–26.2)	13.0 (11.9–14.1)	25.7 (15.7–35.8)	15.8 (15.1–16.5)	14.7 (11.1–18.3)	22.1 (16.6–27.6)	24.0 (9.65–38.3)	21.0 (18.6–23.3)	20.8 (13.0–26.7)
gas-phase PAHs	386 (366–406)	599 (491–707)	370 (289–451)	504 (461–548)	379 (331–428)	335 (317–354)	532 (518–546)	552 (526–580)	655 (643–666)	479 (335–655)
particle-phase PAHs	23.4 (22.0–24.5)	29.7 (24.5–34.8)	8.67 (3.54–13.8)	26.4 (11.0–41.7)	22.7 (16.8–28.6)	19.5 (18.2–20.9)	38.5 (21.1–56.0)	34.7 (13.0–56.5)	17.8 (16.9–18.7)	24.6 (8.67–38.5)
total PAHs	409 (391–428)	629 (516–742)	379 (303–454)	530 (503–559)	402 (359–445)	355 (347–362)	571 (539–602)	587 (582–593)	673 (662–682)	504 (355–673)
total BaP_{eq}	6.77 (6.03–7.51)	5.82 (4.59–7.05)	2.80 (2.47–3.22)	7.41 (4.06–10.8)	4.75 (4.34–5.15)	3.71 (3.20–4.23)	5.86 (5.06–6.66)	6.15 (2.46–9.83)	4.92 (4.08–5.76)	5.35 (2.80–7.41)
total EF_{BaPeq}	28.6 (27.2–30.0)	29.8 (19.9–39.7)	10.9 (8.60–13.1)	34.2 (18.9–49.5)	22.9 (19.7–26.0)	16.3 (15.4–17.2)	22.1 (19.6–24.5)	27.6 (13.6–41.6)	18.0 (14.7–21.4)	23.4 (10.9–34.2)

Table 3. The comparison of PAH profiles, homologues, gas- and particle-phase distributions (range), mean (range) total concentration and EF_{PAHs} obtained from the present study with those data collected from real-scale sinter plants.

PAH emission results	Sinter plants (*7, 31*)	This study
the most abundant compounds	NaP, Ant, AcPy, FL, Flu; [1]NaP, PA, Flu, Fl, Pyr	NaP, AcPy, PA, Flu, FL
homologue in order	2-ring > 3-ring > 4-ring > 5-ring > 6-ring > 7-ring	2-ring > 3-ring > 4-ring > 5-ring > 6-ring > 7-ring
gas- and particle-phase PAHs distribution (%)	Gas = 86 (78–96) Particle = 6.7 (1.3–12.1)	Gas = 95.7 (93.5–98.4) Particle = 4.3 (1.63–6.45)
avg. total PAHs (μg/Nm^3)	778 (555–1001); [1]277	504 (355–673)
avg. total EF_{PAHs} (EF_{PAHs}; μg/kg-feedstock)	3160 (2499–4245)	2364 (1036–3616)

[1] ref. (*31*)

Table 4. The emitted total EF_{BaPeq} (μg/kg-feedstock) and its corresponding S/N ratio (dB) obtained from the reference operation combination and optimal operation combination (including both predicted and that obtained from the confirmation experiments).

testing results		reference operation combination	optimal operation combination	
			prediction	confirmation
Test A	total EF_{BaPeq}	28.6	10.9	-
	S/N ratio	–29.1	–20.5	-
Test B	total EF_{BaPeq}	60.3	-	25.6